

Dear author,

Please note that changes made in the online proofing system will be added to the article before publication but are not reflected in this PDF.

We also ask that this file not be used for submitting corrections.



The chemical behaviour of chlorine in silicate melts

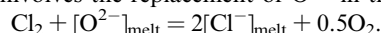
Richard W. Thomas, Bernard J. Wood*

Department of Earth Sciences, University of Oxford, South Parks Road, Oxford OX1 3AN, UK

Received 9 June 2020; accepted in revised form 18 November 2020; available online xxxx

Abstract

We have performed experiments at 0.5–2 GPa and 1200–1500 °C to investigate the dissolution behaviour of chlorine in silicate melts. The experiments were performed with chlorine fugacities controlled by mixtures of Ag, AgCl and AgI and oxygen fugacity buffered at C-CO-CO₂ (CCO) and Re-ReO₂. The results demonstrate that the initial chlorine dissolution mechanism involves the replacement of O²⁻ in the silicate melt by two dissociated Cl⁻ ions according to the reaction:



The same dissolution mechanism applies to hydrous, fluid-saturated basalt at 100–200 MPa/1050 °C. Experiments using both an Fe-free haplobasaltic composition (An₅₀Di₂₈For₂₂) and an Icelandic basalt followed the predicted dependence of Cl concentration on $f(\text{Cl}_2)^{0.5}$ and $f(\text{O}_2)^{0.25}$. This Henrian behaviour extends from 0 to at least 2.6 wt% Cl dissolved in the haplobasaltic composition, 1.6 wt% Cl in anhydrous basalt and ~1.5 wt% Cl in fluid-saturated basalt. Deviations from Henry's Law behaviour at higher concentrations are consistent with progressive association of Cl⁻ ions. In the Henry's Law region Cl concentration in the An₅₀Di₂₈For₂₂ composition is given by (wt%):

$$\log \text{Cl}_{\text{melt}} = 1.206(32) - \frac{940(40)\text{P}}{\text{T}} - 0.25\log(f(\text{O}_2)) + 0.5\log(f(\text{Cl}_2))$$

P is in GPa, T in kelvin, values in brackets are 1 standard error, and $f(\text{Cl}_2)$ and $f(\text{O}_2)$ refer to standard states of pure gas at 0.1 MPa and the temperature of interest. For the natural anhydrous basalt we obtain:

$$\log \text{Cl}_{\text{melt}} = 0.984(64) - \frac{930(70)\text{P}}{\text{T}} - 0.25\log(f(\text{O}_2)) + 0.5\log(f(\text{Cl}_2))$$

By considering the P-T dependences of the Cl contents of melts we find that the concentrations observed in nature are extremely stable in basalt to very low pressures. Basalts containing the typical concentration range of 0.05–0.5 wt% Cl should, for example, only begin to degas their chlorine significantly, as HCl, at pressures in the range 0–5 MPa. Data on hydrous, fluid-saturated basalt at 100–200 MPa are when corrected for dissolution of Ca, Na and K in the fluid, broadly consistent with our results for anhydrous basalt.

Finally, we use recently evaluated thermodynamic data for sodalite (Na₄Al₃Si₃O₁₂Cl) to calculate the conditions under which this phase would stabilise in trachytes and phonolites. We find that the appearance of sodalite as a liquidus phase reflects a combination of low liquidus temperature and high Na₂O activity rather than unusually high chlorine fugacity.

© 2020 Elsevier Ltd. All rights reserved.

Keywords: Chlorine solubility in silicate melts; HCl degassing; Sodalite stability

1. INTRODUCTION

Chlorine is an important volatile component in magmas, exerting significant controls on the properties of silicate melts including diffusion, density, viscosity and phase equilibria (Dingwell and Hess, 1998; Zimova and Webb, 2006; Filiberto and Treiman, 2009a; Baasner et al., 2013).

* Corresponding author.

E-mail addresses: richard.thomas@earth.ox.ac.uk (R.W. Thomas), bernie.wood@earth.ox.ac.uk (B.J. Wood).

<https://doi.org/10.1016/j.gca.2020.11.018>

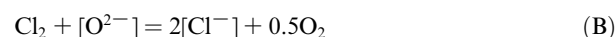
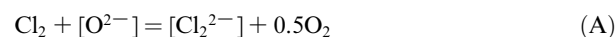
0016-7037/© 2020 Elsevier Ltd. All rights reserved.

Filiberto and Treiman (2009b) have, for example, demonstrated that addition of chlorine to model Martian basalt suppresses the liquidus temperature by amounts comparable, on a weight basis, to those of H₂O. On a molar basis, this means that chlorine has twice as great an effect on liquidus temperature as water. In addition to these effects on melt properties, chlorine is an important ligand in high-temperature hydrothermal fluids, forming soluble complexes with economically important metals such as Cu and Au (Blundy et al., 2015). Volcanogenic chlorine, degassed principally as HCl (Gerlach, 2004) also impacts the atmosphere and hydrosphere, perturbing tropospheric and stratospheric ozone budgets (Bobrowski et al., 2007; Aiuppa et al., 2009), contributing to the development of acid rain, air pollution and the acidification of surficial soils and waters (Aiuppa et al., 2004).

Given its environmental, geochemical and materials importance, the properties and distribution of Cl in natural and experimentally-produced silicate melts and coexisting fluid and vapour phases have been extensively investigated (Webster et al., 2018). In a ground-breaking study, Webster et al. (2015) determined the solubility of Cl in melts ranging from basalt to rhyolite at pressures of 1–7000 bars and 700–1250 °C. This was done by adding chloride salts NaCl, KCl, PtCl₂, PtCl₄, CaCl₂, MgCl₂ and FeCl₂ to the silicate and determining the chlorine contents of the melts at saturation in a hydrosaline liquid with or without vapour (Webster et al., 2015). The data confirm a strong compositional dependence of Cl solubility such that there is a decline of more than an order of magnitude in Cl content as melts evolve from basalt to rhyolite. This study also confirmed earlier results indicating that Cl solubility increases with increasing peralkalinity (Carroll and Webster, 1994; Signorelli and Carroll, 2002; and Evans et al., 2008) and shows strong positive dependences on CaO, MgO and FeO contents. Measured pressure and temperature dependences of Cl solubility appear to depend on the experimental approach taken. In experiments saturated in vapour or high salinity fluid, some data indicate an increase in Cl solubility with decreasing pressure (Shinohara et al., 1989; Métrich and Rutherford, 1992; Signorelli and Carroll, 2002; and Carroll, 2005) while others observe an increase in solubility with increasing pressure (Webster, 1992; Webster et al., 1999; and Webster et al., 2015). Webster et al. (2015) found increases in Cl solubility in equilibrium with hydrosaline liquid with both increasing pressure and increasing temperature. Other authors find a negligible effect of temperature on the solubility of chlorine (Chevychelov et al., 2008; Balcone-Boissard et al., 2016). All of these previous studies depend, however, on the presence of an aqueous fluid or hydrosaline liquid to control the activity of Cl₂ in the silicate melt. In such cases, changes in Cl solubility depend not only on the changing composition of the silicate melt but also on the changing, variable composition of the coexisting fluid or liquid. Our aim here was to avoid this dependence on the nature of the coexisting phase and to buffer Cl contents by an assemblage of known Cl₂ fugacity. In that way, we are able to more accurately define the compositional, pressure and temperature dependences of chlorine concentration in silicate melts.

1.1. Chlorine dissolution in silicate melt

Given the negative charge and the ionic radius of Cl[−] (0.181 nM) it seems likely that this ion substitutes for O^{2−} (ionic radius 0.140 nM, Shannon, 1976) in the silicate framework. This hypothesis was supported experimentally by Bureau et al. (2000) who showed that halogen solubility decreases with the progressive mismatch of the ionic radii of the halide ions (solubility of F > Cl > Br > I), and that of the oxygen ions which dominate the melt structure. The hypothesis of replacement of O^{2−} by Cl[−] leads to two end-member substitution mechanisms:



In equilibria (A) and (B) the nominally charged melt components are represented by brackets [] while the activities of O₂ and Cl₂ are unbracketed. Note that, in both these simplified cases, the solubility of Cl should depend on both the fugacity of Cl₂ and the fugacity of O₂. In equilibrium (A) the Cl[−] ions are assumed to be associated in the melt structure while in equilibrium (B) they are effectively dissociated. Inspection of the equilibrium constants indicates that, in the Henry's Law region, dominance of mechanism (A) should lead to chlorine content of the silicate melt increasing linearly with the fugacity of Cl₂ and decreasing with the square root of oxygen fugacity. In the case of dissociation of the Cl[−] ions (mechanism B), the Cl content of the silicate melt should increase with the square root of the chlorine fugacity and decrease with the fourth root of oxygen fugacity.

Other suggested halogen dissolution mechanisms (e.g. Joachim et al. (2015)) include replacement of an [SiO₄]^{4−} tetrahedron by a [halide]^{4−} quadruplet, and Cl[−] substitution into the O^{2−} site charge-balanced by the substitution of Al³⁺ for Si⁴⁺ (Dalou et al., 2012). In both cases the appropriate charge-balanced equilibria involve both chlorine and oxygen, as well as SiO₂ and Al₂O₃, so that control of both Cl₂ and O₂ fugacities are essential to any experimental test of the proposed mechanism.

It is clear from the preceding discussion that in order to understand the basic chemistry of chlorine dissolution in silicate melt, we need to perform experiments under controlled fugacities of chlorine and oxygen. That was the initial aim of this work.

2. EXPERIMENTAL METHODOLOGY

2.1. Control of chlorine fugacity

We began by following Frantz and Eugster (1973) who developed a chlorine fugacity buffer based on the equilibrium between Ag and AgCl:



Under the conditions of our experiments at 1200–1500 °C and 0.5–2 GPa, we may add metallic Ag and AgCl directly to our silicate melts because Ag₂O is virtually insoluble in the melt. Note that both Ag metal and AgCl are

molten during the high-pressure experiment and that our initial experiments were performed with a silicate melt composition in the system anorthite-diopside-forsterite (Table 1). For equilibrium (1) the fugacity of chlorine is fixed by the equilibrium constant if the Ag metal and AgCl remain pure:

$$f(\text{Cl}_2) = (K_{\text{AgCl}})_{P,T} \quad (2)$$

Thus, we can, in principle, determine the Cl content of the silicate melt at fixed and known chlorine fugacity. We knew from the work of Filiberto and Treiman (2009b) that the Ag/AgCl buffer would release several weight % of Cl into the melt at high pressure and temperature making analysis straightforward with the electron microprobe. In order to investigate the dependence of Cl content on Cl fugacity, we initially expanded the range of Cl fugacities by using other potential buffers Pd-PdCl₂, Re-ReCl₃ and Cu-CuCl. In practice, we find that all 4 of the potential buffers control the chlorine fugacity at too high values for the basalt-like compositions we have used. The evidence for this statement is the generation of immiscible chloride 'blobs' rich in Ca and Mg during the experiment with concomitant decreases in the CaO and MgO contents of the coexisting silicate melt (Fig. 2b) and Cl contents of the latter of up to 9 wt%.

In order to suppress the formation of chloride blobs, we reduced the chlorine fugacity by mixing the AgCl with either AgBr or AgI. We found that high ratios of AgI:AgCl was the best option because the solubility of I (<0.1 wt%) in melts is much lower than that of Br (up to 1.65 wt%). During the experiment the Ag and AgCl/AgI mixtures both melt to form 2 additional liquids (metal and halide) both of which are immiscible with one another and with the silicate melt.

Most experiments used an anorthite–diopside–forsterite (An₅₀Di₂₈For₂₂) mixture, which is close to the 1.5 GPa eutectic in the system CaO–MgO–Al₂O₃–SiO₂ (Presnall et al., 1978) and is hence an Fe-free model of a low degree mantle melt. The starting composition was prepared from a mixture of analytical grade oxide powders and CaCO₃. The mixture was decarbonated by heating overnight from 500 to 1100 °C. A second series of experiments was performed using a crushed and powdered natural basalt from Reykjanes Ridge, Iceland (Norris and Wood, 2017; Table 1). Finally, because the experiments on the natural basalt expe-

rienced, for reasons which are as yet unclear, various degrees of Fe loss to the Pt capsule, we examined the effects of FeO concentration by performing three experiments in which various amounts (3, 7 and 10 wt%) of synthetic Fe_{1-x}O were intimately mixed with our buffer-An₅₀Di₂₈For₂₂ mixes.

Experiments were performed with anhydrous silicates (Table 1) in an end-loaded 'Boyd and England'-type ½ inch piston-cylinder apparatus (Boyd and England, 1960) at the University of Oxford. Starting compositions of intimate mixtures of silicate and chlorine buffer were loaded into capsules, the configuration of which depended on the required oxygen fugacity (Fig. 1). The Pt outer capsules were welded shut and weighed prior to the experiment.

The experiments employed a 32 mm long, 12.5 mm outside diameter, 8 mm inside diameter calcium fluoride cylinder as the principal pressure medium. Inside this cylinder was an 8 mm O.D., 6 mm I.D. graphite cylinder which acts as the furnace. The 3 mm outside diameter capsule (Fig. 1) was placed in the centre of the graphite furnace with crushable MgO pieces above, below and around the capsule. The temperature was measured and controlled using an alumina-sheathed C-type (W₉₅Re₅–W₇₄Re₂₆) thermocouple, introduced through a hole in the upper MgO piece and separated from the capsule by a 0.5 mm thick alumina disc. Experiments were performed at 1200–1500 °C and 0.5–2.0 GPa (Table 2) using the 'hot piston-in' method and the pressure calibrations of McDade et al. (2002) for ≥1.0 GPa, and Vlach et al. (2019) for <1.0 GPa. Experimental durations, mostly 1 h, were based on a time-series performed to test for the approach to equilibrium (see below; Fig. 3). All experiments were quenched by cutting the power to the graphite furnace (cooling at ≈110 °C/s). Once extracted, the recovered capsule was cleaned, weighed and compared to pre-experimental measurements to ensure no mass was lost or gained during the experiment.

2.2. Control of oxygen fugacity

We tested our ability to control oxygen fugacity at the CCO buffer using the $f(\text{O}_2)$ sensor model of Kessel et al. (2001) at 1350 °C and 1.5 GPa. This model uses activity-composition relations of Pt-Fe alloys in conjunction with silicate activities as follows:

$$\log f(\text{O}_2) = \log \left\{ \exp \left[\ln a_{\text{Fe}_2\text{SiO}_4}^{\text{liq}} - \ln a_{\text{SiO}_2}^{\text{liq}} - 2 \ln a_{\text{Fe}}^{\text{alloy}} - \left(\frac{-\Delta G_r^0}{RT} \right) \right] \right\} \quad (3)$$

where ΔG_r^0 is the standard state free energy change for the reaction $2\text{Fe}^{\text{alloy}} + \text{O}_2^{\text{gas}} + \text{SiO}_2^{\text{liq}} = \text{Fe}_2\text{SiO}_4^{\text{liq}}$

The model employs the MELTS supplementary calculator (Ghiorso and Sack, 1995) to calculate the activities of SiO₂ and Fe₂SiO₄ components in the complex liquid.

An experimental assembly was created using two graphite capsules within the outer Pt capsule. In the upper capsule, the powdered Icelandic basalt (Table 1) was added with a small Pt bead. In the bottom capsule, Ag₂CO₃ and graphite powder were added to form the C–CO–CO₂ (CCO) buffer, given, as follows from Jakobsson and Oskarsson (1994):

Table 1

Silicate melt compositions used for measuring chlorine solubility.

Composition	CMAS (An ₅₀ Di ₂₈ For ₂₂) ^a	Icelandic Basalt ^b
SiO ₂	46.53	50.76
TiO ₂	–	1.02
Al ₂ O ₃	18.33	15.32
FeO	–	9.61
MgO	17.82	9.19
CaO	17.33	12.26
Na ₂ O	–	2.01

^a 1.5 GPa approximate eutectic composition (Presnall et al., 1978).

^b Natural Icelandic Basalt (Norris and Wood, 2017).

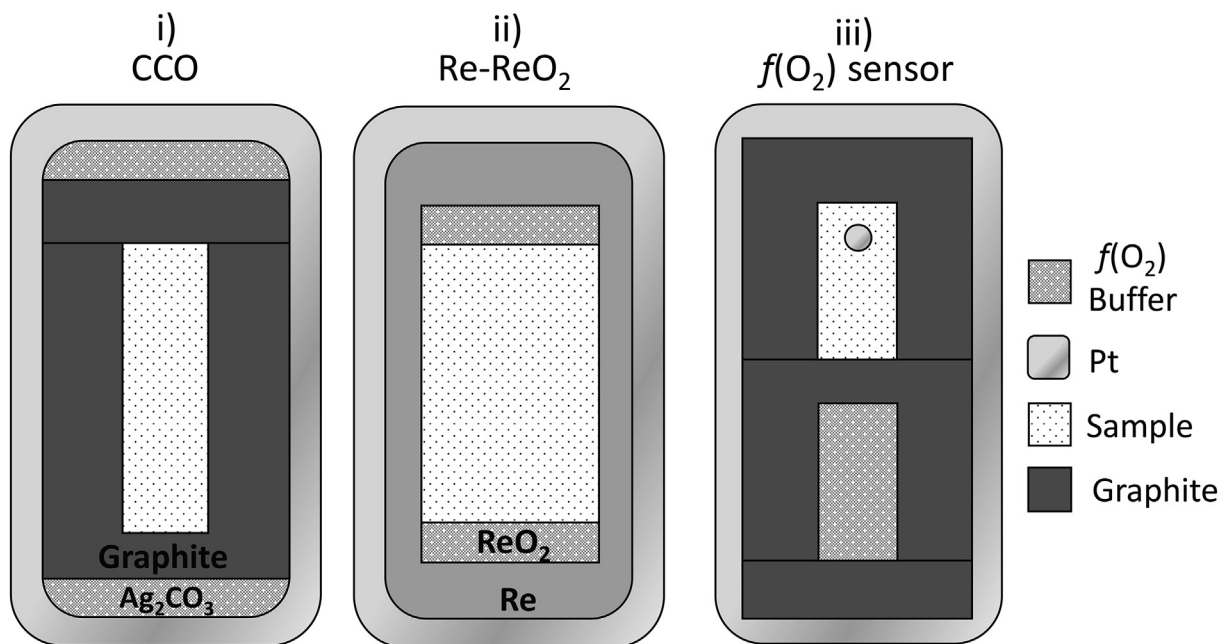


Fig. 1. Capsule assemblies (i) CCO buffered experiments. Mixtures of chlorine buffer (Ag/AgCl/AgI) plus silicate were packed into 2.5 mm O.D., 1 mm I.D. graphite capsules encapsulated in a Pt capsule of 2.5 mm I.D and 3.0 mm O.D. Ag_2CO_3 (source of CO_2) added above and below the graphite capsule and Pt outer capsule welded shut. (ii) Re-Re O_2 buffered experiments. ReO_2 powder packed above and below the silicate-chlorine buffer mixture inside 2.5 mm (O.D) Re foil capsule within a welded outer Pt capsule. (iii) Assembly to check $f(\text{O}_2)$. Lower graphite capsule with a CO_2 source and upper with iron-bearing sample (IB, Table 1) and a small Pt bead.

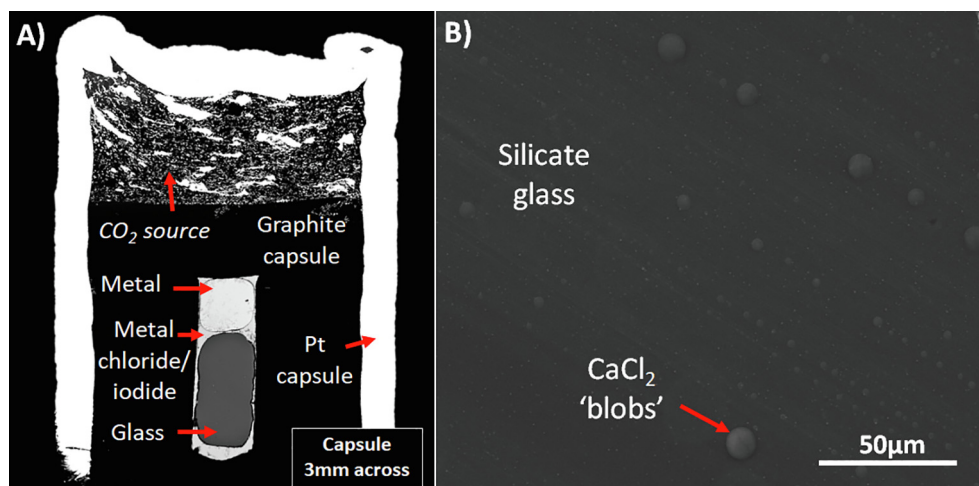


Fig. 2. (A) Back-Scattered Electron (BSE) image of a typical experimental product, displaying (1) CO_2 source and (2) Separate and distinct phases of silicate glass, metal chloride/iodide and metal. (B) BSE image of silicate glass displaying immiscible chloride 'blobs' rich in Ca and Mg which exsolve from the silicate melt at high chlorine fugacities. BSE images were taken on the FEI Quanta 650 at the University of Oxford's Department of Earth Sciences.

$$\log f(\text{O}_2)(\text{CCO}) = 4.325 - \left(\frac{21803}{T} \right) + 0.171 \left(\frac{(P-1)}{T} \right) \quad (4)$$

Analysis of the bead after the experiment yielded a mol fraction of 0.31 Fe (11.34 wt%) in the Pt and 5.22 wt% FeO in the silicate melt which indicates an oxygen fugacity 1.79 log units below the FMQ buffer. Taking the latter from Frost (1991):

$$\log f(O_2) \text{ (FMQ)} = \left(\frac{-25096.3}{T} \right) + 8.735 + 0.11 \left(\frac{(P-1)}{T} \right) \quad (5)$$

This is within 0.03 of the expected value, 1.82 log units below FMQ and so we can be confident that our oxygen fugacity is fixed at CCO.

In order to determine the effect of oxygen fugacity on the Cl content of the silicate melt, we performed additional experiments using the Re-ReO₂ oxygen buffer. We lined the Pt capsule with Re foil and added ReO₂ in layers on the top and bottom of the charge (Fig. 1). The oxygen fugacity is given by Pownceby and O'Neill (1994):

$$\log f(O_2) \text{ (RRO)} = \frac{(-451020 + 297.595T - 14.6585T \ln T)}{RT \ln 10} + \left(\frac{0.9917P}{RT \cdot 303} \right) \quad (6)$$

Note that pressure in Eqs. (4)–(6) is in bars.

Attempts to use additional anhydrous oxygen buffers have so far proven unsuccessful. A Mo-MoO₂ mixture released too much Mo into the silicate (~36 wt%), and pure oxygen (from PtO₂) oxidised the Ag buffer which dissolved ~24 wt% Ag₂O into the melt.

2.3. Analytical techniques

During the experiment, the buffer-silicate mixture segregated into a homogeneous translucent glass, a metal chloride/iodide phase and an Ag-rich metal alloy (Fig. 2a). The capsules were mounted in epoxy, ground to expose the charge and polished with diamond powder using toluene or mineral oil as a lubricant to prevent any Cl loss to water-based lubricants. From a check on the potential for Cl-loss, however, we found, in agreement with Mungall and Brenan (2003) that two samples re-polished with water-based lubricant showed no measurable loss of Cl.

Product silicate glasses and chlorine fugacity buffers were analysed on the CAMECA SX-Five-FE at the University of Oxford's Department of Earth Sciences and the JEOL-8600 electron microprobe in the University of Oxford's Archaeology department. The results obtained from each instrument were used to check for inconsistencies and levels of precision and accuracy. A 20 nA beam current, 15 kV accelerating voltage and a defocused 10 μm beam diameter was used for the glass analysis. To minimise the potential for element migration during analysis, Cl, Na, and Si were analysed first with the 10 μm defocused beam. Standards used for silicate glass analysis were natural albite (Si, Al, Na), andradite (Ca, Fe), Titanium dioxide (Ti) Thallium-bromide-iodide (Br, I), synthetic NaCl crystals (Cl), periclase (Mg) and pure metals of Pt, Re, and Ag. Counting times were a minimum of 30 s peak and 15 s background for all elements except for Cl for which 80 s peak and 40 s background were used to obtain a detection

limit of 120 ppm. Replicate analysis on the same spots of glass revealed that Cl counts were stable and consistent at these conditions; with over 40 points on each silicate portion of the charge, and 10–20 points within the remaining buffer and resultant metal phases. Results remained consistent with low (<0.2 wt%) standard deviations (Table 2); secondary standards including Durango and Bamble apatite, containing known concentrations of Cl of 0.41 wt% (Kusebauch et al., 2015a) and 7.09 wt% (Kusebauch et al., 2015b) respectively were used to ensure accurate Cl analysis. In the case of Durango apatite (0.41 wt% Cl) we obtained an average of 0.415 wt% Cl with standard deviation of 0.015% for 98 analyses performed over the duration of the study.

3. RESULTS

All experimental run conditions, the concentrations of chlorine in the resultant glass phases and calculated chlorine fugacities are given in Table 2. Complete analyses of the silicate glass products are presented in supplementary Table 1.

3.1. Attainment of equilibrium

We performed a time series from 5 min to 2 h at 1400 °C/1.5 GPa with oxygen fugacity fixed at the CCO buffer and chlorine fugacity provided by an initial AgI:AgCl ratio of 75:25 by weight. The concentration of Cl in the glass rose and levelled off after 5 min, with within-error variation between experiments performed at 0.5–2 h, and negligible difference between 1 and 2 h (2.55 and 2.56 wt% Cl respectively; Table 2; Fig. 3. Most further experiments were therefore performed for 1 h (Table 2).

3.2. Calculation of chlorine fugacity $f(\text{Cl}_2)$ under experimental conditions

With both Ag metal and AgCl present as liquids in equilibrium, the fugacity of chlorine is calculated from the equilibrium constant (K) for reaction (1). The equilibrium constant was obtained at one bar from thermodynamic data of Barin et al. (1989):

$$\log (K)_{1\text{bar}} = 11440/T - 2.961 \text{ (1000–1800 K)} \quad (7)$$

which yields if both Ag and AgCl are pure:

$$\log f(\text{Cl}_2) = -11440/T + 2.961 \quad (8)$$

We use a 0.1 MPa standard state for Cl₂ and standard states for Ag and AgCl as the pure liquids at the pressure and temperature of interest. This means we need to integrate ΔVdP for the metal and chloride liquids from 1 bar to the pressure of interest. The volume of AgCl liquid is known to about 1123 K (31.95 cm³), so we chose to integrate at this temperature. To a good approximation, we can express volume (V) as a function of pressure (P) by:

$$V_{PT} = V_{1T}(1 - bP) \quad (9)$$

Table 2
Experimental conditions and compositions.

Experiment	Silicate composition	Time (mins)	Temperature (°C)	Pressure (GPa)	$f(\text{O}_2)$ buffer	$\log f(\text{O}_2)$	Measured Cl^{glass} wt%	FeO wt% in melt	Buffer/Silicate by mass	Initial weight ratio $\text{Cl}/(\text{Cl} + \text{I})$	Final Molar $\text{Cl}/(\text{Cl} + \text{I})$	Molar $\text{Ag}/(\text{Ag} + \text{Pt})$	$f(\text{Cl}_2)$
Time series													
AgI/Cl-007	CMAS	5	1400	1.5	CCO	−7.17	2.24 (0.05)	–	75/25	0.353	0.220	0.924	3.37E−04
AgI/Cl-002	CMAS	30	1400	1.5	CCO	−7.17	2.74 (0.14)	–	75/25	0.353	0.183	0.837	2.82E−04
AgI/Cl-005	CMAS	60	1400	1.5	CCO	−7.17	2.55 (0.04)	–	75/25	0.353	0.198	0.844	3.24E−04
AgI/Cl-006	CMAS	120	1400	1.5	CCO	−7.17	2.56 (0.07)	–	75/25	0.353	0.198	0.861	3.11E−04
$f(\text{Cl}_2)$ series													
AgI/Cl-018	CMAS	60	1400	1.5	CCO	−7.17	0.18 (0.01)	–	65/35	0.032	0.014	0.856	1.66E−06
AgI/Cl-010	CMAS	60	1400	1.5	CCO	−7.17	0.21 (0.01)	–	90/10	0.032	0.017	0.864	2.29E−06
AgI/Cl-009	CMAS	60	1400	1.5	CCO	−7.17	0.50 (0.03)	–	90/10	0.079	0.045	0.869	1.59E−05
AgI/Cl-008	CMAS	60	1400	1.5	CCO	−7.17	1.02 (0.03)	–	80/20	0.154	0.082	0.851	5.43E−05
AgI/Cl-005	CMAS	60	1400	1.5	CCO	−7.17	2.55 (0.04)	–	75/25	0.353	0.198	0.844	3.24E−04
AgI/Cl-013	CMAS	60	1400	1.5	CCO	−7.17	3.59 (0.09)	–	50/50	0.621	0.407	0.843	1.38E−03
AgI/Cl-027	ICB	60	1400	1.5	CCO	−7.17	1.60 (0.03)	0.5 (0.13)	50/50	0.353	0.209	0.778	4.24E−04
AgI/Cl-023	ICB	60	1400	1.5	CCO	−7.17	0.77 (0.06)	3.24 (0.89)	80/20	0.154	0.100	0.799	9.32E−05
AgI/Cl-037	ICB	60	1400	1.5	CCO	−7.17	0.41 (0.09)	1.67 (0.17)	90/10	0.079	0.052	0.823	2.31E−05
AgI/Cl-039	ICB	60	1400	1.5	CCO	−7.17	0.32 (0.01)	2.6 (0.18)	60/40	0.079	0.038	0.793	1.36E−05
$f(\text{O}_2)$ series													
AgI/Cl-029	CMAS	60	1400	1.5	RRO	−3.75	0.69 (0.04)	–	75/25	0.353	0.317	0.742	1.08E−03
AgI/Cl-031	ICB	60	1400	1.5	RRO	−3.75	0.33 (0.02)	3.48 (0.1)	50/50	0.353	0.329	0.823	9.45E−04
Temperature series													
AgI/Cl-028	CMAS	60	1500	1.5	CCO	−6.52	2.66 (0.07)	–	75/25	0.353	0.189	0.786	6.72E−04
AgI/Cl-005	CMAS	60	1400	1.5	CCO	−7.17	2.55 (0.04)	–	75/25	0.353	0.198	0.844	3.24E−04
AgI/Cl-020	CMAS	420	1300	1.5	CCO	−7.90	2.41 (0.16)	–	75/25	0.353	0.208	0.931	1.38E−04
AgI/Cl-043	ICB	60	1500	1.5	CCO	−6.52	1.77 (0.09)	8.52 (0.13)	50/50	0.353	0.189	0.702	8.44E−04
AgI/Cl-027	ICB	60	1400	1.5	CCO	−7.17	1.60 (0.03)	0.5 (0.13)	50/50	0.353	0.209	0.778	4.24E−04
AgI/Cl-044	ICB	3	1300	1.5	CCO	−7.90	1.52 (0.02)	1.15 (0.08)	50/50	0.353	0.217	0.814	1.97E−04
AgI/Cl-045	ICB	31	1200	1.5	CCO	−8.73	1.48 (0.17)	8.19 (0.36)	50/50	0.353	0.222	0.832	8.30E−05
Pressure series													
AgI/Cl-032	CMAS	60	1400	0.5	CCO	−8.20	3.39 (0.04)	–	75/25	0.353	0.128	0.909	1.09E−05
AgI/Cl-019	CMAS	60	1400	1	CCO	−7.68	2.93 (0.04)	–	75/25	0.353	0.169	0.858	7.46E−05
AgI/Cl-005	CMAS	60	1400	1.5	CCO	−7.17	2.55 (0.4)	–	75/25	0.353	0.198	0.844	3.24E−04
AgI/Cl-021	CMAS	60	1400	2	CCO	−6.66	2.12 (0.03)	–	75/25	0.353	0.229	0.830	1.20E−03
AgI/Cl-051	CMAS	60	1400	1	CCO	−7.68	1.23 (0.03)	–	80/20	0.154	0.065	0.865	1.07E−05
AgI/Cl-008	CMAS	60	1400	1.5	CCO	−7.17	1.02 (0.03)	–	80/20	0.154	0.082	0.851	5.43E−05
AgI/Cl-052	CMAS	120	1400	2	CCO	−6.66	0.81 (0.02)	–	80/20	0.154	0.097	0.852	2.05E−04
AgI/Cl-050	ICB	60	1400	0.5	CCO	−8.20	2.19 (0.11)	8.24 (0.15)	50/50	0.353	0.140	0.879	1.37E−05
AgI/Cl-048	ICB	60	1400	1	CCO	−7.68	2.05 (0.12)	7.57 (0.17)	50/50	0.353	0.156	0.821	6.95E−05
AgI/Cl-027	ICB	60	1400	1.5	CCO	−7.17	1.60 (0.03)	0.5 (0.13)	50/50	0.353	0.209	0.778	4.24E−04
AgI/Cl-049	ICB	150	1400	2	CCO	−6.66	1.62 (0.14)	8.22 (0.19)	50/50	0.353	0.206	0.657	1.55E−03

Fe-bearing CMAS											
60	1400	1.5	CCO	-7.17	2.54 (0.06)	8.68 (0.19)	75/25	0.353	0.198	0.887	2.96E-04
60	1400	1.5	CCO	-7.17	2.7 (0.19)	15.69	75/25	0.353	0.184	0.864	2.46E-04
						(0.46)					
60	1400	1.5	CCO	-7.17	3.49 (0.28)	20.88	75/25	0.353	0.120	0.903	1.04E-04
						(0.49)					

CI% error in () is 2 stdev.

where b is the isothermal compressibility, of 0.101 per GPa at 801 K (Marcus, 2013). Taking account of the temperature dependence of the adiabatic compressibility from Takeda et al. (2007) implies isothermal compressibility of approximately 0.13/GPa at 1123 K.

For Ag liquid, the volume at the 1-atmosphere melting point of 1233 K is 11.49 cm³. Taking thermal expansion, volume and compressibility from [Tsu et al. \(1982\)](#) yields a volume of 11.37 cm³, and *b* of 0.0146/GPa at 1123 K by metastable extrapolation. Integrating between 0.1 MPa and *P* and adding in the ΔV_{dP} terms leads to:

$$\log f(\text{Cl}_2) = -11440/T + 2.961 + 2150P/T - 208P^2/T \quad (10)$$

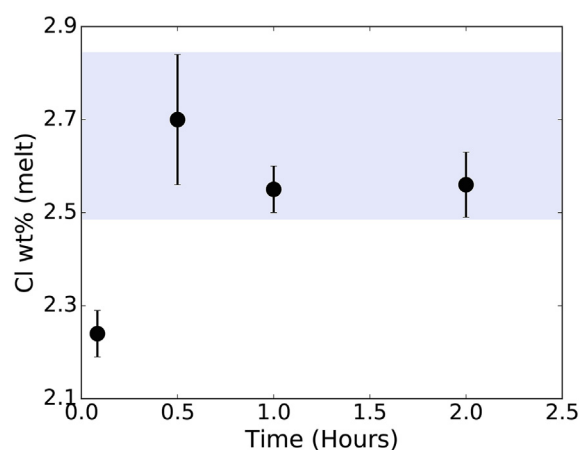


Fig. 3. Chlorine concentration in $\text{An}_{50}\text{Di}_{28}\text{Fo}_{22}$ melt as a function of time at 1400 °C, 1.5 GPa and at the CCO oxygen buffer. Buffer contained AgI:AgCl of 75:25 (Table 2).

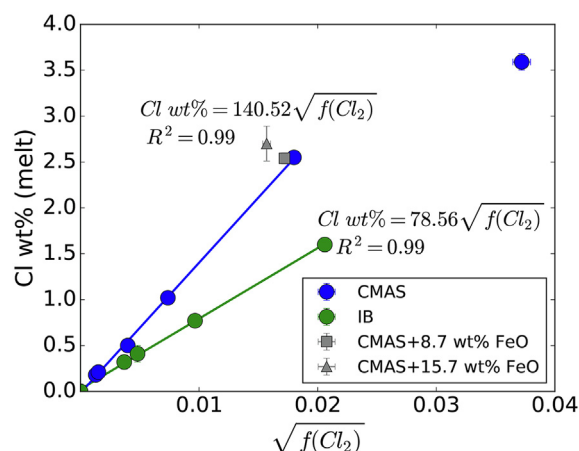


Fig. 4. Chlorine concentration in the melt at 1400 °C and 1.5 GPa plotted as a function of the square root of chlorine fugacity with oxygen fugacity buffered at CCO. CMAS refers to $\text{An}_{50}\text{Di}_{25}\text{Fo}_{22}$ composition and IB to Icelandic basalt. Experiments performed with CMAS + FeO are denoted in grey, and 8.68 wt% FeO and 15.69 wt% FeO refer to wt%FeO in the product glasses.

In Eq. (10) P is in GPa and, as before, the fugacity of chlorine refers to the value for pure Ag in equilibrium with pure AgCl and is relative to a standard state of pure chlorine at 0.1 MPa and the temperature of interest.

As discussed earlier, we found that use of the Ag/AgCl buffer with pure AgCl led to exsolution of a separate chloride phase rich in Ca and Mg (Fig. 2b) and a corresponding change in major element composition of the silicate melt. In order to suppress this effect, we diluted the AgCl with, initially AgBr and then with AgI until there was no separate Ca-Mg chloride phase and no measurable reduction in the ratios of Ca and Mg to Si in the product silicate glass. We then reduced the AgCl/AgI ratio further to develop a range of chlorine fugacities at fixed pressure, temperature and oxygen fugacity. In adopting this procedure, we adjusted the ratios of chlorine buffer to silicate to ensure that the amount of Cl remaining in the buffer could be accurately calculated by mass-balance.

By diluting the liquid AgCl with AgI (or AgBr), we decrease chlorine fugacity by an amount approximately proportional to the square of the ratio $\text{Cl}/(\text{Cl} + \text{I})$. Additionally, we found that there was some Ag-Pt exchange between the metal of the capsule and that of the buffer. From the Ag-Pt phase diagram (Hart et al., 2017) we anticipate a mole fraction of Ag in the Ag-rich alloy of ~ 0.75 – 0.85 and values close to this were observed in all experiments (Table 2). In the absence of thermochemical mixing data for metal and halide liquids, we corrected for the effects of impurities by assuming ideal solution in both AgCl-AgI and Ag-Pt liquids. This yields:

$$\log f(\text{Cl}_2) = \log f(\text{Cl}_2^{\text{pure AgCl}}) + 2\log(X_{\text{Cl}}) - 2\log(X_{\text{Ag}}) \quad (11)$$

In Eq. (11) X_{Cl} refers to $\text{Cl}/(\text{Cl} + \text{I})$ in the halide liquid and X_{Ag} to $\text{Ag}/(\text{Ag} + \text{Pt})$ in the metal liquid on a molar basis (Table 2).

3.3. Chlorine solubility as a function of chlorine fugacity, $f(\text{Cl}_2)$

7 experiments were conducted on our CMAS composition at 1.5 GPa, 1400 °C, using the CCO oxygen buffer (Fig. 1). To examine the effects of variable FeO concentration, we also performed experiments in which 3, 7 and 10 wt % Fe_{1-x}O were added to the starting mix of buffer plus CMAS. A similar series of 5 experiments were performed under identical conditions using the natural basalt as a starting composition. By adjusting the ratios of AgI to AgCl, and of buffer to silicate melt we were able to vary the fugacity of chlorine over the range from 0 to 1.38×10^{-3} bar (Table 2 and Fig. 4). Chlorine fugacities in Table 2 were calculated from the final $\text{Cl}/(\text{Cl} + \text{I})$ of the buffer mixture, which was determined by mass-balancing Cl concentration in the silicate glass with Cl content of the initial mixture. We assumed an initial weighing uncertainty of $\pm 2\%$ relative to generate the error bars of Fig. 4a and b.

In Fig. 4 we plot the Cl contents of the two melts versus the square root of chlorine fugacity. Fig. 4 demonstrates

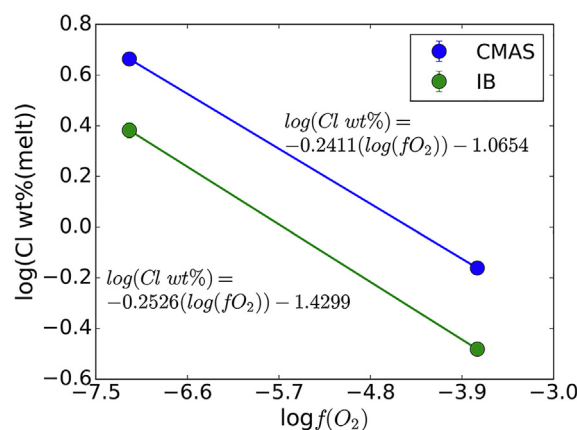


Fig. 5. $\log(\text{Cl wt\% melt})$ as a function of oxygen fugacity, $\log(f(\text{O}_2))$ at 1400 °C and 1.5 GPa. Chlorine concentrations were corrected to a fixed $f(\text{Cl}_2)$ by extrapolation from the Henrian region (Fig. 4). Chlorine concentration should decrease with the fourth root of $f(\text{O}_2)$ between CCO (-7.17) and Re-ReO₂ (-3.75) oxygen buffers if 2Cl^- ions replace O^{2-} in the melt.

clearly that the Cl contents of the melts are linear functions of $f(\text{Cl}_2)^{0.5}$ to concentrations of >2.6 wt% Cl. This constitutes Henry's Law behaviour of constant activity coefficient. Above a point in the range 2.6–3.6 wt% Cl behaviour becomes non-Henrian, but the Henrian region is extensive. The clear linear dependence of Cl content on $f(\text{Cl}_2)^{0.5}$ in the region 0–2.6% Cl indicates that Cl dissolves according to reaction (B), with two dissociated Cl^- ions replacing O^{2-} . At higher concentrations, the observed deviation (Fig. 4) would be consistent with progressive association of Cl^- ions. It is also worth noting that addition of 8.7 wt% FeO to the CMAS composition produces a negligible change in Cl content and that the Cl concentration of melt with 15.7 wt% FeO added changes from 2.55 wt% (FeO-free) to 2.7 wt% (Fig. 4). The observed $f(\text{Cl}_2)$ -dependence means that we can exclude the proposed halogen dissolution mechanism in which an $[\text{SiO}_4]^{4-}$ tetrahedron is replaced by a $[\text{halide}]^{4-}$ quadruplet since this would lead to a dependence of Cl concentration on $f(\text{Cl}_2)^2$.

Both compositions tested obey a Henrian relationship with increasing $\sqrt{f(\text{Cl}_2)}$. However, Cl solubility in Icelandic basalt is lower at fixed Cl_2 fugacity than in the haplobasalt, indicating a significant compositional dependence of the Henry's Law constant. This compositional dependence is clearly not due to variable FeO content in the range 0–10 wt% (Fig. 4). Since, in addition to FeO, the largest compositional differences between our 2 compositions are in their CaO and MgO contents we believe that these 2 components are largely responsible for the enhanced Cl content of the CMAS composition. This suggestion is consistent with the Cl solubility model of Webster et al. (2015) which is based on lower pressure experiments saturated in hydrosaline liquids and which indicates strong positive dependences of Cl solubility on CaO and MgO contents of the melt. In order to test our model of replacement of O^{2-} by 2 dissociated Cl^- ions, we turned to the dependence of chlorine solubility on oxygen fugacity.

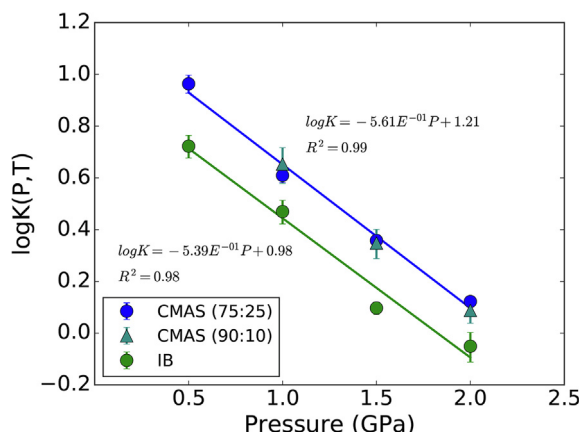


Fig. 6. Plot of $\log K$ for the reaction: $0.5\text{Cl}_2 + 0.5[\text{O}^{2-}]_{\text{melt}} = [\text{Cl}^-]_{\text{melt}} + 0.25\text{O}_2$ as a function of pressure at 1400 °C. Experiments performed with oxygen fugacity at CCO. CMAS refers to $\text{An}_{50}\text{Di}_{28}\text{Fo}_{22}$ composition and (75:25) and (90:10) refer to weight percentages of AgI and AgCl in the buffer. IB refers to the Icelandic basalt of Table 1.

3.4. Oxygen fugacity $f(\text{O}_2)$

We explored the effect of oxygen fugacity on chlorine solubility using $f(\text{O}_2)$ buffers CCO and Re-ReO₂, in both natural Icelandic basalt and haplobasaltic compositions (Table 1).

In order to quantify the effect of oxygen fugacity on Cl solubility, we need to correct the data to a constant chlorine fugacity. We did this by extrapolating the linear Henry's Law region determined from the experiments at the CCO buffer in each composition (Fig. 4) to the point where the chlorine fugacity was the same as in our experiments at the Re-ReO₂ buffer. Once corrected in this way, it is apparent that chlorine solubility decreases, from 2.41 wt% to 0.33 wt%; and 4.61 wt% to 0.69 wt% (for ICB and CMAS compositions respectively) with increasing oxygen fugacity (Fig. 5). The change in $\log f(\text{O}_2)$ from RRO (−3.75) to CCO (−7.17) at 15,000 bars and 1400 °C is −3.42. If Cl dis-

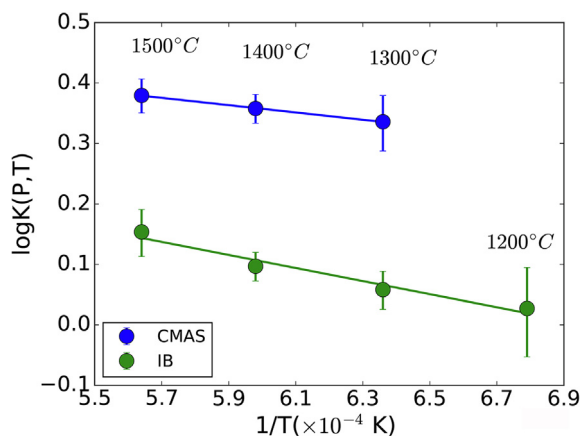


Fig. 7. Plot of $\log K$ for the reaction: $0.5\text{Cl}_2 + 0.5[\text{O}^{2-}]_{\text{melt}} = [\text{Cl}^-]_{\text{melt}} + 0.25\text{O}_2$ versus $1/T$ at 1.5 GPa. Symbols as in Fig. 6.

solution follows reaction (B), chlorine concentration should decrease with the fourth root of $f(\text{O}_2)$. This means that the concentration at Re-ReO₂ should be 0.14 times the concentration at CCO. Our observed values are 0.15 times and 0.135 times for CMAS and ICB compositions, respectively. This consistency between predicted and observed $f(\text{O}_2)$ -dependences leads us to conclude that reaction (B) represents the principal mechanism by which chlorine (and presumably other halogens) dissolves in silicate melts. We will, therefore, continue our treatment on this basis.

3.5. The effects of pressure and temperature on chlorine solubility

Experiments were conducted over a pressure range from 0.5 to 2 GPa, at a constant temperature of 1400 °C, and held at the CCO buffer, using both CMAS and Icelandic basalt compositions with similar Cl/(Cl + I) contents of the buffer (25:75 AgCl to AgI by weight). Although raw results indicate a decrease in Cl concentration in the melt with increasing pressure we need to correct-out the pressure effects on the Cl and oxygen buffers in order to determine the true pressure effect. This was done by correcting the Cl concentration in the melt to a constant ratio of $f(\text{Cl}_2)^{0.5}; f(\text{O}_2)^{0.25}$ following the stoichiometry of reaction (B). Correcting this way allows us to express the pressure effect as (Fig. 6):

$$\frac{\partial \log K}{\partial P} = \frac{-\Delta V^0}{2.303RT} \quad (12)$$

where ΔV^0 is the volume change of reaction, R is the gas constant ($8.3145 \text{ J K}^{-1} \text{ mol}^{-1}$), T is the temperature in Kelvin, P is pressure and the equilibrium constant, K is given by:

$$\log K_{(P,T)} = \log([\text{Cl}^-] + 0.25 \log(f(\text{O}_2)) - 0.5 \log(f(\text{Cl}_2))) \quad (13)$$

In Eq. (13), $[\text{Cl}^-]$ is the concentration of chlorine in the silicate melt in weight %. Once these corrections are applied, similar negative correlations of $\log K$ with pressure are observed for both compositions at 1400 °C (Fig. 6). The slope yields for ΔV^0 in the CMAS composition:

$$\Delta V^0 = -(-5.61E^{-4} * 2.303RT) = 17.8 \text{ cm}^3 \cdot (\text{gm} \cdot \text{atom})^{-1} \quad (14)$$

The basalt composition yields ΔV^0 of 17.3 cm^3 per gm atom. This volume change corresponds to the difference between the effective volumes of ICl^- and 0.5O^{2-} in the melt and would be expected to approximate half the volume difference between, for example, CaCl_2 and CaO ($17.03 \text{ cm}^3/\text{mol}$) or MgCl_2 and MgO ($14.78 \text{ cm}^3/\text{mol}$) (Robie et al., 1979). The agreement provides further support for our dissolution model (see Fig. 7).

We performed experiments at 100 °C intervals between 1300 and 1500 °C for the CMAS composition and 1200–1500 °C for the basalt composition, in both cases at 1.5 GPa with oxygen fugacity buffered at CCO, and similar Cl/(Cl + I) contents of the buffer (25:75 AgCl to AgI by weight). We fitted the results for each composition by step-

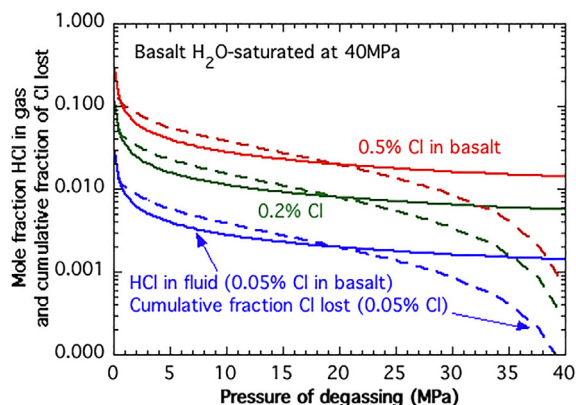


Fig. 8. Shows calculated HCl contents (mole fraction) of gases emitted by basalt at its liquidus temperature as a function of pressure of degassing (solid lines). Curves refer to different Cl contents (wt %) of the basalt. Gas was assumed to contain 5 mol% each of C and S species with the balance H_2 , H_2O and HCl. Also shown (dashed lines) are cumulative fractions of total Cl degassed from an H_2O -saturated basalt at 40 MPa (2 wt% H_2O) during ascent to the surface. All results are independent of oxygen fugacity (see text).

wise regression using the multiple linear regression tool of the SPSS statistical package. The appropriate fit equation is:

$$\log K_{(P,T)} = \log(Cl^-) + 0.25 \log(f(O_2)) - 0.5 \log(f(Cl_2))$$

$$= A - B/T - CP/T \quad (15)$$

We found, however, that the B/T term in Eq. (15) does not pass the F-test at the normal level ($\alpha = 0.05$) requiring α of 0.2 in the CMAS composition and 0.9 in the basalt. This term was therefore excluded from the fit with the following result for the CMAS composition:

$$\log K_{P,T}^{CMAS} = \log(Cl^-) + 0.25 \log(f(O_2)) - 0.5 \log(f(Cl_2))$$

$$= 1.206(32) - 940(40)P/T \quad (16)$$

and for the basalt:

$$\log K_{P,T}^{basalt} = \log(Cl^-) + 0.25 \log(f(O_2)) - 0.5 \log(f(Cl_2))$$

$$= 0.984(64) - 930(70)P/T \quad (17)$$

In Eqs. (16) and (17) P is in GPa, T in kelvin, (Cl^-) is the Cl content of the melt in weight% and the numbers in brackets are the standard errors in the 2 fit parameters. The standard errors of the fits are 0.030 and 0.053 in $\log K$, respectively.

4. DISCUSSION

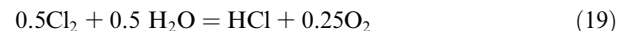
4.1. Chlorine fugacity and gas composition on the basalt liquidus

The range of Cl concentrations in basalt glasses from the Mid-Ocean-Ridges and Back-Arc Basins typically extends

from ~0.01 to 0.5 wt% with occasional values above the latter figure (Webster et al., 2018). In order to illustrate the implications of these concentrations for chlorine fugacity and evolved gas composition, we started by assuming oxygen fugacities at FMQ (Cottrell and Kelley, 2011) and calculated chlorine fugacities from Eq. (17) for Cl contents of 0.05, 0.2 and 0.5 wt%. We assumed temperatures at the MORB liquidus of Médard and Grove (2008):

$$T(^{\circ}C) = 1267 + 65 \times P(GPa) \quad (18)$$

We then calculated the composition of C-O-H-S-Cl gases which would be evolved from basalt at its liquidus temperature at shallow levels in the crust (Fig. 8). For illustration, we assumed 5 mol% each of C and S species with the remainder H_2 , H_2O and HCl. Thermodynamic data for the gas species were taken from Barin et al. (1989). Oxygen fugacity was fixed at FMQ with chlorine fugacity obtained from the fixed Cl content of the melt as described above. We used the 2-parameter Modified Redlich Kwong (MRK) equation of state with parameters for CO_2 , H_2O , CO , H_2 and CH_4 from Holloway (1977), as modified by Flowers (1979). Data for HCl, H_2S and SO_2 were taken from Prausnitz et al. (1999). It should be noted, however, that because temperatures are high and pressures low, fugacity coefficients are close enough to 1 in the illustrated range for a perfect gas assumption to have given reasonable results. It is also important to note that the results of Fig. 8 are actually independent of oxygen fugacity in the region where HCl is the dominant form of Cl in the gas phase. This is because, in an H_2O -rich fluid, the reaction controlling the HCl fugacity is:



Inspection of reaction (19) shows that, at fixed H_2O fugacity, the HCl fugacity depends on the ratio of $f(Cl_2)^{0.5}/f(O_2)^{0.25}$. Since this is exactly the same dependence

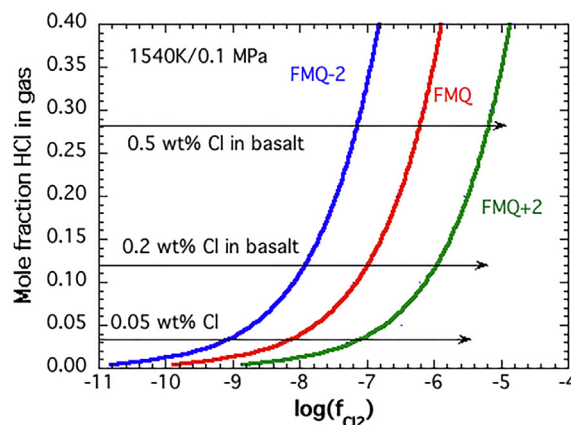


Fig. 9. Shows relationships between Cl_2 fugacity, O_2 fugacity and gas composition (mole fraction of HCl) for basalt at its liquidus temperature and a pressure of 0.1 MPa. Note that for fixed Cl content of basalt (horizontal lines labelled in wt% Cl) the mole fraction of HCl is independent of Cl_2 and O_2 fugacities. HCl contents and Cl_2 fugacities covary along the lines labelled at oxygen fugacities relative to FMQ, the fayalite-magnetite-quartz buffer.

on the ratio of chlorine to oxygen fugacity as the Cl content of the melt (equilibrium B), any change in oxygen fugacity, at fixed Cl content of the melt, is cancelled-out by a corresponding change in chlorine fugacity.

As can be seen from Fig. 8, Cl is calculated to degas significantly from basaltic melts and presumably from most other melts only at very shallow depths. Even for melts containing 0.5 wt% Cl, a C–O–H–S–Cl fluid evolved at 40 MPa would only contain an HCl mole fraction of 0.016. At 1 MPa the HCl mole fraction would be 0.10 and at 0.1 MPa 0.28. Thus, we would predict that HCl would degas only in the very uppermost parts of a volcanic edifice or during an eruption. This is consistent with the observations of Edmonds et al. (2009) who found that S degasses at Kilauea at a greater depth than HCl and that the latter only degases at depths of 35 meters or less, pressures below 10 MPa. Similarly, at Soufrière Hills, Montserrat, Edmonds et al. (2001) and Christopher et al. (2015) found that hydrous andesitic melts degas HCl at low pressures within the upper parts of the conduit system and during an eruption. Additionally, Aiuppa (2009) found that halogens only appreciably degassed during syn-eruptive, or late-stage degassing of residual magmas from Etna and Stromboli.

As a further illustration of the retention of Cl by the melt, even at very low pressure, we considered an H₂O-saturated basalt at 1269 °C and 40 MPa and calculated, using HCl concentrations in the evolved gas, the total amount of Cl lost during ascent to the surface from this pressure. The water-saturated basalt initially has 2 wt% H₂O, and the degassing path was calculated using VolatileCalc2.0 (Newman and Lowenstern, 2002). As can be seen in Fig. 8, the total fraction of the Cl degassed at pressures >5 MPa is extremely small for all 3 concentrations of Cl considered. Eruption at the surface, with all H₂O lost, would lead to 98% of the original Cl remaining in the liquid if it had contained 0.05 wt% Cl initially, 93% if it originally contained 0.2 wt% Cl and 84% if it initially contained 0.5 wt% Cl i.e. 0.42 wt% Cl would remain in the liquid at 0.1 MPa.

The reason that HCl degasses only at very low pressures, given the very high solubility of Cl in silicate melts can be seen from inspection of reaction (19). The equilibrium constant for the reaction depends on the ratio of fugacities $f_{\text{HCl}}/f_{\text{H}_2\text{O}}^{0.5}$. Since fugacities at these pressures are virtually identical to partial pressure, we can replace them by pressure and mole fractions X_{HCl} and $X_{\text{H}_2\text{O}}$:

$$\frac{f(\text{HCl})}{f_{\text{H}_2\text{O}}^{0.5}} = \text{constant} \cong \frac{P X_{\text{HCl}}}{(P X_{\text{H}_2\text{O}})^{0.5}} \quad (20)$$

From Eq. (20), we see that with increasing pressure, the ratio $X_{\text{HCl}}:X_{\text{H}_2\text{O}}$ in the fluid, at fixed Cl content of the melt, decreases with the square root of pressure as observed in Fig. 8.

In Fig. 9, we present the calculated 0.1 MPa HCl contents of gases in equilibrium with basalt as functions of $f(\text{O}_2)$ and $f(\text{Cl}_2)$. As noted previously, the HCl concentrations depend only on the concentrations of Cl in the silicate melts, provided, as calculated from thermodynamic data, the HCl contents of the gases are very much greater than

the Cl₂ concentrations. So, for example, a gas in equilibrium with basalt containing 0.5 wt% Cl has a mole fraction X_{HCl} of 0.28, independent of oxygen fugacity and chlorine fugacity. The concentration of 0.5 wt% Cl defines a line in $f(\text{O}_2)$ – $f(\text{Cl}_2)$ space; however, as can be seen in Fig. 9. Thus at FMQ, the log $f(\text{Cl}_2)$ associated with 0.5% Cl in the melt is –6.3, while a decrease or increase of $f(\text{O}_2)$ by 2 log units decreases or increases $f(\text{Cl}_2)$ by 1 log unit.

4.2. HCl solubility in basaltic melts

In volcanic systems in which evolved gases are dominated by H₂O, the observed form of chlorine is HCl (Gerlach, 2004) and HCl is predicted, from thermodynamic data, to dominate over Cl₂ under all plausible conditions of H₂O content and oxygen fugacity. Given these observations and predictions, it is of interest to compare our results with the data of Iwasaki and Katsura (1967) who measured the concentration of Cl in basalt (also andesite and rhyolite) equilibrated with mixtures of HCl and N₂ at 1-atmosphere pressure and temperatures of 1200–1290 °C. At 1290 °C, Iwasaki and Katsura found an HCl solubility of 1.06 wt% in basalt at 0.1 MPa of HCl pressure, 0.22 wt% at 0.01 MPa and 0.1 wt% at 0.003 MPa of HCl pressure. We used the saturation limit of 1.06 wt% HCl in the melt at 0.1 MPa of HCl pressure Eq. (16) to calculate the ratio $f(\text{Cl}_2)/f(\text{O}_2)^{0.5}$ for a basalt containing 1.03 wt% Cl (equivalent to 1.06 wt% HCl). We then used (19) and (20) to calculate the composition of an HCl–H₂O gas which would be in equilibrium with this Cl content of basalt. We obtain a gas, at 0.1 MPa, which has an HCl partial pressure of 0.084 MPa effectively very close to the experimental value of 0.1 MPa. Alternatively, we can calculate the H₂ fugacity required to produce the measured Cl contents at known HCl fugacity. For all 3 measured HCl contents, we find that, if the HCl gas flowing through the furnace contained plausible H₂ contamination of less than 0.0001 (i.e. >0.9999 HCl, <0.0001 H₂) we can reproduce the measured HCl con-

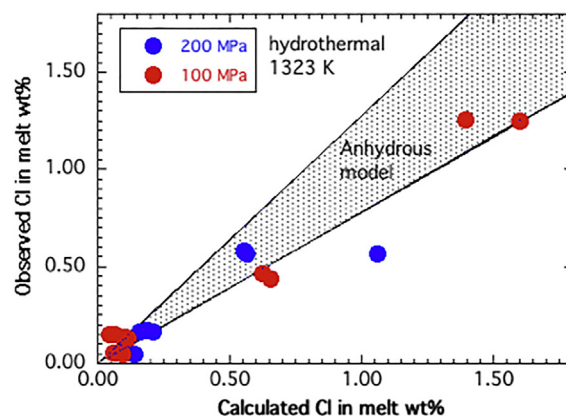


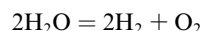
Fig. 10. Plot of Cl contents of hydrous basalts in equilibrium with excess fluid at 100–200 MPa/1050 °C (Beermann et al., 2015) versus values calculated from the compositions of the fluids using our anhydrous basalt model (Eq. (17)). The field labelled “anhydrous model” covers ± 2 standard errors of the fit to our anhydrous data.

tents of the glasses from our solubility model. The agreement appears to us to be acceptable.

4.3. Hydrous melts in equilibrium with Cl-bearing fluids

Beermann et al. (2015) have determined the partitioning of Cl between hydrous basaltic melts and Cl-bearing aqueous fluids at 1050 °C and pressures of 100 and 200 MPa. The method used by these authors involved the addition of an H₂O–HCl liquid to a basalt glass starting material to which small amounts of sulphur had been added. The starting composition was calculated to contain about 5–6% excess fluid. Experiments in sealed gold capsules were performed in an internally-heated pressure vessel under conditions where the H₂ fugacity was controlled by a “Shaw”-membrane or measured using such a membrane. Glass composition was measured after the experiment and fluid composition reconstructed from the glass composition and the initial composition. The results indicate that Cl substitution in the hydrous melts follows Henry’s Law, consistent with our proposed substitution mechanism (B) to concentrations of at least 1 wt% Cl in the melt. Of even greater interest is an estimate of how closely the Cl contents of these hydrous melts follow our anhydrous basalt model of Eq. (17)

We used the H₂ pressures and H₂O concentrations quoted by Beermann et al. (2015) to calculate O₂ fugacities from the equilibrium:

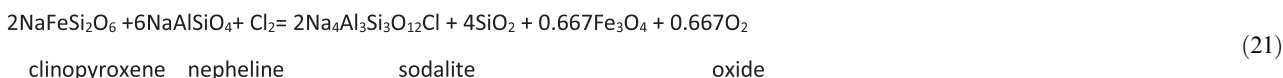


Cl contents of the melts calculated as if the melts were anhydrous. Results were not adjusted upwards to correct for the H₂O contents of the melts (2.7–7.5 wt%).

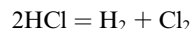
Fig. 10 shows a comparison of calculated and measured Cl contents of the melts in the concentration range in which Henry’s Law is closely obeyed (0–1.5 wt% Cl approx). As can be seen, when uncertainties in our results are considered, virtually all data are in agreement with the anhydrous model, which, given the potential errors and uncertainties is encouraging. It implies that hydrothermal and anhydrous results can be connected to one another in a relatively straightforward way.

4.4. Stability of Sodalite in trachytes and phonolites

Although Cl is a minor component of igneous apatite and amphibole, the principal phase in which it is a major component is sodalite, nominally Na₄Al₃Si₃O₁₂Cl which is a primary precipitating phase in some peralkaline trachytes and phonolites. We consider it instructive to calculate the chlorine fugacities required to stabilise sodalite in trachytes and compare them with the values we have obtained for basalts (Fig. 9). Stormer and Carmichael (1971) estimated the free energy of sodalite from the experiments of Wellman (1969) and calculated the conditions under which sodalite would be stable relative to nepheline and other silicates. In order to calculate the chlorine fugacity required to stabilise sodalite, they used the equilibrium:



We calculated H₂ and H₂O fugacities at the pressure and temperature of each experiment using the MRK equation of state as described above and used thermodynamic data of Barin et al. (1989) to calculate $f(\text{O}_2)$. Since Beermann et al., observed appreciable dissolution of Ca, Na and K from the melt into the fluid we followed their Fig. 10 and assumed that 25% of the Cl in the fluid was complexed as Ca, Na or K chlorides. The remaining Cl contents of the fluids were allocated to HCl and $f(\text{Cl}_2)$ calculated from thermodynamic data (Barin et al., 1989) for the equilibrium:



As before, we used the MRK equation of state for H₂ and HCl and calculated chlorine fugacities relative to the 0.1 MPa standard state. The calculated oxygen and chlorine fugacities were then inserted into Eq. (17) and the expected

This was applied to a lava (W158) from Mt. Suswa, Kenya in which sodalite coexists with nepheline, plagioclase, olivine, clinopyroxene and oxide. Coexistence of nepheline and albitic plagioclase enables calculation of SiO₂ activity while the activities of Fe₃O₄, NaFeSi₂O₆ and NaAlSiO₄ together with oxygen fugacity were calculated from the compositions of oxide, olivine clinopyroxene and nepheline determined by Nash et al. (1969). The calculation presented by Stormer and Carmichael indicates that extremely low Cl₂ fugacities ($\sim 10^{-16}$ at 1300 K/1 bar) are required to stabilise sodalite in trachytic lavas. This value is about 8 orders of magnitude lower than the typical chlorine fugacities implied by the Cl contents of basaltic magmas at their liquidus temperatures (Fig. 9). It is, however, based on experiments in which gas pressures over decomposing sodalite at 1 atm were measured (Wellman, 1969) and is based on the assumption of equilibrium between

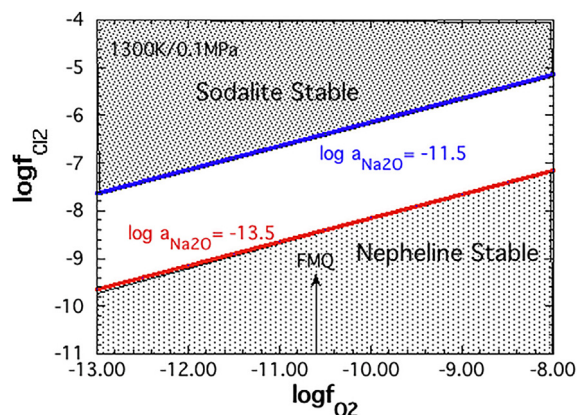
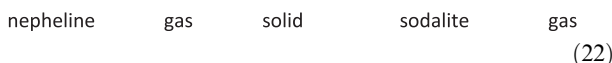
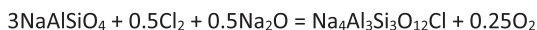


Fig. 11. Calculated stability of sodalite relative to nepheline as a function of Cl_2 and O_2 fugacities at 1300 K and 0.1 MPa. The calculated Na_2O activity in trachyte is $\sim 10^{-12.5}$ and the lines at $10^{-11.5}$ and $10^{-13.5}$ are intended to provide a reasonable estimate of uncertainty. FMQ = fayalite-magnetite-quartz oxygen buffer.

sodalite and its decomposition products nepheline and NaCl gas. Sharp et al. (1989) showed, however, that Wellman's experiments dramatically overestimate the stability of sodalite and therefore that the requisite chlorine fugacities for sodalite stability must be much higher than implied by the earlier data.

In a recent paper, Wood et al. (2019) used Sharp et al.'s (1989) high-pressure experimental reversals of the breakdown of sodalite to β -nepheline plus solid NaCl together with the heat capacity and third law entropy measurements of Komada et al. (1995) to obtain the free energy of sodalite in the temperature range 300–1000 K. We extended the temperature range of sodalite free energy data by taking account of the experimental reversals at 1073 K (0.78–0.80 GPa) and 1173 K (0.84–0.86 GPa). These enable us to make calculations of chlorine fugacity in the 1-atmosphere liquidus-solidus interval of trachyte.

In order to calculate the chlorine fugacities necessary to stabilise sodalite in trachytes and phonolites we used the equilibrium:



We took thermodynamic data from Barin et al. (1989) combined with our free energy of sodalite, to calculate the free energy change of (22). For the experimental temperature range of 800–1175 K and 0.1 MPa pressure we obtain, for equilibrium (22):

$$\log K_{22} = -0.526 + 10710/T \quad R^2 = 0.9999 \quad (23)$$

For comparison with earlier results, we have extrapolated the data slightly and perform the following calculations at 1300 K.

At 1300 K and 0.1 MPa pressure $\log K_{22}$ is 7.71. In order to calculate the ratio $f(\text{Cl}_2)/f(\text{O}_2)^{0.5}$ required to stabilise sodalite, given nepheline saturation, we need to know the activity of Na_2O in the melt, relative to a standard state

of pure solid Na_2O . We derived Na_2O activity from the MELTS thermodynamic model of Ghiorso and Sack (1995). In order to do this, we used the MELTS supplemental calculator to calculate activities of Na_2SiO_3 and SiO_2 in the melts of interest. We then calculated the activity of Na_2O from the equilibrium:



Melt solid melt

We tested the validity of this approach by using the MELTS supplementary calculator to calculate Na_2O activities in melts in the system $\text{Na}_2\text{O}-\text{Al}_2\text{O}_3-\text{SiO}_2$ studied by Itoh and Yokokawa (1984) at 1400 K. The latter authors measured Na_2O activities relative to the solid standard state we use in equilibrium (22). At 1400 K, we obtain an Na_2O activity of $10^{-9.3}$ from MELTS for the composition 20 Na_2O :80 SiO_2 (mole%) as compared to an experimental value of $10^{-9.5}$. For aluminous compositions $\text{Na}_2\text{O}:\text{Al}_2\text{O}_3:\text{SiO}_2$ of 20:10:70, 20:5:75 and 25:5:70 we obtain respectively, experimental values in parentheses- $10^{-9.2}$ ($10^{-9.0}$), $10^{-9.3}$ ($10^{-9.2}$) and $10^{-8.3}$ ($10^{-8.9}$). This demonstrates that the MELTS approach should yield reasonable values of Na_2O activity for mildly peralkaline silicate liquids.

We calculated the activity of Na_2O in 3 trachytes (W158 discussed above, W120 and W227) from Mt. Suswa, Kenya analysed by Nash et al. (1969). At 1300 K, we obtained between $10^{-12.5}$ and $10^{-12.6}$ for all 3 liquids using the MELTS software. Note that we changed the standard state free energies of Na_2SiO_3 and SiO_2 liquids slightly to be consistent with Barin's (1989) data but that this increases Na_2O activities only slightly, by about 0.1 log units.

Given the calculated Na_2O activity in trachyte of about $10^{-12.5}$ at 1300 K, we are able to apply equilibrium (22) to calculate the conditions under which sodalite would be stabilised in such a melt. We assumed, following Nash et al. (1969) that the typical nepheline would be about 75% NaAlSiO_4 and allowed it to be an ideal solution. We then constructed lines of equilibrium $\log f(\text{Cl}_2)$ versus $\log f(\text{O}_2)$ for equilibrium between sodalite and nepheline according to (22). Sodalite is stable at high $f(\text{Cl}_2)$ and nepheline at low $f(\text{Cl}_2)$, as shown in Fig. 11. This figure shows that, as anticipated, the chlorine fugacity required to stabilise sodalite is much higher (~ 9 orders of magnitude) than that calculated by Stormer and Carmichael (1971). For illustration, we allow a liberal uncertainty of ± 1 log units in Na_2O activity since this is larger than the difference between any of the calculated values and the experiments discussed above and construct lines in $\log f(\text{Cl}_2):\log f(\text{O}_2)$ space at Na_2O activities of $10^{-11.5}$ and $10^{-13.5}$ (Fig. 11). As can be seen from Fig. 11, the Cl_2 fugacities required to stabilise sodalite in trachyte at FMQ/1300 K are of the order of $10^{-6.8}$ to $10^{-8.8}$, almost exactly the same as those required to dissolve 0.05–0.5 wt % Cl in basalt at 1540 K (Fig. 9). For comparison, Nash et al. (1969) note that the sodalite-bearing lavas of Mt. Suswa contain, in their centres 0.25–0.5 wt% Cl whereas glassy, sodalite-free lavas contain < 0.25 wt% Cl. The implications are that the Cl_2 fugacities and the HCl contents of gases in equilibrium with basalt containing 0.5 wt% Cl are similar to those in equilibrium with trachyte containing 0.5 wt% Cl. Whether this is coincidence or indicates a rela-

tively small dependence of Cl content on melt composition in the range basalt-trachyte is as yet unknown.

5. CONCLUSIONS

Our experiments have demonstrated that chlorine initially dissolves in silicate melts by a mechanism in which one oxygen anion is replaced by 2 dissociated chloride, Cl^- ions. The same mechanism applies to both anhydrous and hydrous basaltic melts. We find that dissolution behaviour follows Henry's Law (constant ratio of concentration to $f(\text{Cl}_2)^{0.5}$) from zero to concentrations of at least 2.6 wt% Cl in a haplobasalt of composition $\text{An}_{50}\text{Di}_{28}\text{Fo}_{22}$ and at least 1.6 wt% Cl in an Icelandic basalt (Table 1, Fig. 4) both at 1400 °C. At fixed temperature, pressure and fugacities of chlorine and oxygen; however, the Cl concentration in the FeO-free composition is 1.7 times that in the Icelandic basalt (Fig. 4, Eqs. (16) and (17)). In the case of hydrous basalt at 1050 °C Henry's Law is obeyed to ~1.5 wt% Cl and Cl contents are similar to values predicted from the anhydrous basalt data.

We performed experiments to determine whether the difference in Cl contents of our two anhydrous compositions is due to the presence of FeO in the natural basalt. Addition of 8.68 wt% FeO to the $\text{An}_{50}\text{Di}_{28}\text{Fo}_{22}$ composition melt made, however, negligible difference to the Cl content of 2.55 wt%. Even addition of 15.69 wt% FeO only raised the Cl content, under equivalent conditions of pressure, temperature and fugacities of chlorine and oxygen from 2.55 to 2.7%. We conclude that variations in FeO content in the range 0–10 wt% should not generate measurable differences in equilibrium Cl content of a silicate melt.

At high Cl fugacities, generated by Ag/AgCl mixtures without AgI addition, we observed losses of CaO and MgO into immiscible chloride 'blobs' (Fig. 1). We therefore, consider it probable that the major compositional factors controlling the differences in Cl dissolution between our two compositions are CaO and MgO concentrations, both of which act to increase the equilibrium Cl content. From the pressure dependence of Cl content at fixed fugacities of chlorine and oxygen, we find that the difference in volume between 1Cl^- ion and 0.5O^{2-} in silicate melt is 17.3–17.8 cm^3/mol . This compares well with half the volume difference between crystalline CaCl_2 and CaO of 17.03 cm^3/mol .

Our data enable us to calculate chlorine fugacities in basalt as a function of pressure, temperature and composition. Given that Cl predominantly degasses from silicate melt as HCl, we used our equation for Cl content and Cl fugacity, (17), to calculate the HCl contents of gases released from basaltic melt as a function of pressure in the upper crust (Fig. 8). This figure shows that basalts containing the typical concentration range of 0.05–0.5 wt% Cl degas little of their Cl at 25–30 MPa (800–900 meters depth) with chlorine being largely retained until pressures are below 5 MPa. The strong pressure dependence of equilibrium HCl contents is due to the fact that when H_2O interacts with Cl in the melt 2 molecules of HCl are produced for every molecule of H_2O consumed (Eq. (19)). This results in

a large increase in volume, an effect which causes HCl release to be reduced as pressure increases.

At FMQ and 0.1 MPa, the range of equilibrium chlorine fugacities implied by a basalt containing 0.5–0.05% Cl is $10^{-6.3}$ to $10^{-8.3}$ (Fig. 9). This value increases by 1 log unit for every 2 log units increase in oxygen fugacity. We addressed the changes in Cl_2 fugacity likely to be observed in nature by calculating the conditions under which the Cl-rich phase sodalite would become stable near the liquidus in alkaline trachytes or phonolites. We calculate, based on thermodynamic data for sodalite, that this phase would be stable at 1300 K/0.1 MPa and oxygen fugacities at the FMQ buffer if chlorine fugacities were $10^{-6.8}$ to $10^{-8.8}$ (Fig. 11). There appears, therefore, to be little difference in chlorine fugacities represented by alkaline trachytes at their liquidus and basalts at their liquidus. Appearance of sodalite as a liquidus phase is probably, therefore, due to a combination of low temperature and high Na_2O activity rather than unusually high chlorine fugacity.

UNCITED REFERENCES

Lowenstern (2000), Malinin et al. (1989), Stelling et al. (2008), Webster (2004), Webster and Holloway (1988), Webster and De Vivo (2002).

Declaration of Competing Interest

The authors declare that they have no known competing financial interests or personal relationships that could have appeared to influence the work reported in this paper.

ACKNOWLEDGEMENTS

RWT is grateful to the National Environmental Research Council, and the Oxford Doctoral Training Partnership in Environmental Research for studentship and funding (NE/L002612/1). BJW acknowledges funding from Science and Technology Facilities Council grant ST/R000999/1 and the NERC FAMOS project NE/P017452/1 project. We acknowledge the thorough reviews of 2 anonymous reviewers and Dr. Z. Zajacz.

APPENDIX A. SUPPLEMENTARY MATERIAL

Supplementary data to this article can be found online at <https://doi.org/10.1016/j.gca.2020.11.018>.

REFERENCES

- Aiuppa A. (2009) Degassing of halogens from basaltic volcanism: insights from volcanic gas observations. *Chem. Geol.* **263**, 99–109.
- Aiuppa A., Baker D. R. and Webster J. D. (2009) Halogens in volcanic systems. *Chem. Geol.* **263**, 1–18.
- Aiuppa A., Federico C., Giudice G., Gurrieri S., Paonita A. and Valenza M. (2004) Plume chemistry provides insights into mechanisms of sulfur and halogen degassing in basaltic volcanoes. *Earth Planet. Sci. Lett.* **222**, 469–483.

- Baasner A., Schmidt B. C. and Webb S. L. (2013) The effect of chlorine, fluorine and water on the viscosity of aluminosilicate melts. *Chem. Geol.* **357**, 134–149.
- Balcone-Boissard H., Boudon G., Cioni R., Webster J. D., Zdanowicz G., Orsi G. and Civetta L. (2016) Chlorine as a geobarometer for alkaline magmas: evidence from a systematic study of the eruptions of Mount Somma-Vesuvius. *Sci. Rep.* **6**.
- Barin I., Sauert F., Schultze-Rhonhof E. and Sheng W. S. (1989) Thermochemical data of pure substances: Part II.
- Beermann O., Botcharnikov R. E. and Nowak M. (2015) Partitioning of sulfur and chlorine between aqueous fluid and basaltic melt at 1050°C, 100 and 200 MPa. *Chem. Geol.* **418**, 132–157.
- Blundy J., Mavrogenes J., Tattitch B., Sparks S. and Gilmer A. (2015) Generation of porphyry copper deposits by gas-brine reaction in volcanic arcs. *Nat. Geosci.* **8**, 235–240.
- Bobrowski N., von Glasow R., Aiuppa A., Inguaggiato S., Louban I., Ibrahim O. W. and Platt U. (2007) Reactive halogen chemistry in volcanic plumes. *J. Geophys. Res.* **112**, 1–17.
- Boyd F. R. and England J. L. (1960) Apparatus for phase-equilibrium measurements at pressures up to 50 kilobars and temperatures up to 1750°C. *J. Geophys. Res.* **65**, 741–748.
- Bureau H., Keppler H. and Métrich N. (2000) Volcanic degassing of bromine and iodine: experimental fluid/melt partitioning data and applications to stratospheric chemistry. *Earth Planet. Lett.* **189**, 51–60.
- Carroll M. R. (2005) Chlorine solubility in evolved alkaline magmas. *Ann. Geophys.* **48**, 619–631.
- Carroll M. R. and Webster J. D. (1994) Solubilities of sulfur, noble gases, nitrogen, chlorine, and fluorine in magmas. *Mineral. Soc. Am. Rev. Mineral.* **30**, 231–279.
- Chevychev V., Bocharnikov R. E. and Holtz F. (2008) Experimental study of chlorine and fluorine partitioning between fluid and subalkaline basaltic melt. *Dokl. Earth Sci.* **422**, 93–97.
- Christopher T. E., Blundy J., Cashman K., Cole P., Edmonds M., Smith P. J. and Sparks R. S. J. (2015) Crustal-scale degassing due to magma system destabilization and magma-gas decoupling at Soufrière Hills Volcano, Montserrat. *Geochim. Geophys. Geosyst.* **16**, 267–300.
- Cottrell E. and Kelley K. A. (2011) The oxidation state of Fe in MORB glasses and the oxygen fugacity of the upper mantle. *Earth Planet. Sci. Lett.* **305**, 270–282.
- Dalou C., Koga K. T., Nobumichi S., Boulon J. and Devidal J.-L. (2012) Experimental determination of F and Cl partitioning between lherzolite and basaltic melt. *Contrib. Mineral. Petrol.* **163**, 591–609.
- Dingwell D. B. and Hess K. U. (1998) Melt viscosities in the system Na-Fe-Si-O-F-Cl: contrasting effects of F and Cl in alkaline melts. *Am. Mineral.* **83**, 1016–1021.
- Edmonds M., Gerlach T. M. and Herd R. A. (2009) Halogen degassing during ascent and eruption of water-poor basaltic magma. *Chem. Geol.* **263**, 122–130.
- Edmonds M., Pyle D. and Oppenheimer C. (2001) A model for degassing at the Soufrière Hill Volcano, Montserrat, West Indies, based on geochemical data. *Earth Planet. Sci. Lett.* **186**, 159–173.
- Evans K. A., Mavrogenes J. A., O'Neill H. S., Keller N. S. and Jang L. Y. (2008) A preliminary investigation of chlorine XANES in silicate glasses. *Geochim. Geophys. Geosyst.* **9**, 1–15.
- Filiberto J. and Treiman A. H. (2009a) Martian magmas contained abundant chlorine, but little water. *Geology* **37**, 1087–1090.
- Filiberto J. and Treiman A. H. (2009b) The effect of chlorine on the liquidus of basalt: first results and implications for basalt genesis on Mars and Earth. *Chem. Geol.* **263**, 60–68.
- Flowers G. C. (1979) Correction of Holloway's (1977) adaptation of the modified Redlich-Kwong equation of state for calculation of the fugacities of molecular species in supercritical fluids of geologic interest. *Contrib. Mineral. Petrol.* **69**, 315–318.
- Frantz J. D. and Eugster H. P. (1973) Acid-base buffers: Use of Ag + AgCl in the experimental control of solution equilibria at elevated pressures and temperatures. *Am. J. Sci.* **273**, 268–286.
- Frost R. B. (1991) Introduction to oxygen fugacity and its petrologic importance. *Rev. Mineral. Geochem.* **25**, 1–9.
- Gerlach T. M. (2004) Volcanic sources of tropospheric ozone-depleting trace gases. *Geochim. Geophys. Geosyst.* **5**, 1–16.
- Ghiorso M. S. and Sack R. O. (1995) Chemical mass transfer in magmatic processes IV. A revised and internally consistent thermodynamic model for the interpolation and extrapolation of liquid-solid equilibria in magmatic systems at elevated temperatures and pressures. *Contrib. Mineral. Petrol.* **119**, 197–212.
- Hart G. L. W., Nelson L. J., Vanfleet R. R., Campbell B. J., Sluiter M. H. F., Neethling J. H., Olivier E. J., Allies S., Lang C. I., Meredig B. and Wolverton C. (2017) Revisiting the revised Ag-Pt phase diagram. *Acta Mater.* **124**, 325–332.
- Holloway J. R. (1977) Fugacity and activity of molecular species in supercritical fluids. In *Thermodynamics in Geology* (ed. D. G. Fraser). D. Reidel Publishing Company, Dordrecht, pp. 161–181.
- Itoh H. and Yokokawa T. (1984) Thermodynamic activity of Na₂O in Na₂O-SiO₂-Al₂O₃ melt. *Trans. Japan Inst. Met.* **25**, 879–884.
- Iwasaki B. and Katsura T. (1967) The solubility of hydrogen chloride in volcanic rock melts at a total pressure of one atmosphere and at temperatures of 1200°C and 1290°C under anhydrous conditions. *Bull. Chem. Soc. Jpn.* **40**, 554–561.
- Jakobsson S. and Oskarsson N. (1994) The system C-O in equilibrium with graphite at high pressure and temperature: an experimental study. *Geochim. Cosmochim. Acta* **58**, 9–17.
- Joachim B., Pawley A., Lyon I. C., Marquardt K., Henkel T., Clay P. L., Ruzié L., Burgess R. and Ballentine C. J. (2015) Experimental partitioning of F and Cl between olivine, orthopyroxene and silicate melt at Earth's mantle conditions. *Chem. Geol.* **416**, 65–78.
- Kessel R., Beckett J. R. and Stolper E. M. (2001) Thermodynamic properties of the Pt-Fe system. *Am. Mineral.* **86**, 1003–1014.
- Komada N., Westrum E. F., Hemingway B. S., Zolotov M. Y., Semenov Y. V., Khodakovskiy I. L. and Anovitz L. M. (1995) Thermodynamic properties of sodalite at temperatures from 15 K to 1000 K. *J. Chem. Thermodyn.* **27**, 1119–1132.
- Kusebauch C., John T., Whitehouse M. J., Klemme S. and Putnis A. (2015a) Distribution of halogens between fluid and apatite during fluid-mediated replacement processes. *Geochim. Cosmochim. Acta* **170**, 225–246.
- Kusebauch C., Timm J., Whitehouse M. J. and Engvik A. K. (2015b) Apatite as probe for the halogen composition of metamorphic fluids (Bamble Sector, SE Norway). *Contrib. Mineral. Petrol.* **170**.
- Lowenstern J. B. (2000) A review of the constraining behaviour of two magmatic volatiles: chlorine and Carbon dioxide. *J. Geochemical Explor.* **69–70**, 287–290.
- Malinin S. D., Kravchuk I. F. and Delbove F. (1989) Chloride distribution between phases in hydrated and dry chloride-aluminosilicate melt systems as a function of phase composition. *Geochim. Perspect. Lett.* **26**, 32–36.
- Marcus Y. (2013) The compressibility of molten salts. *J. Chem. Thermodyn.* **61**, 7–10.
- McDade P., Wood B. J., Van Westrenen W., Brooker R., Gudmundsson G., Soular H., Najorka J. and Blundy J. (2002) Pressure corrections for a selection of piston-cylinder cell assemblies. *Mineral. Mag.*

- Médard E. and Grove T. L. (2008) The effect of H₂O on the olivine liquidus of basaltic melts: experiments and thermodynamic models. *Contrib. Mineral. Petrol.* **155**, 417–432.
- Métrich N. and Rutherford M. J. (1992) Experimental study of chlorine behavior in hydrous silicic melts. *Geochim. Cosmochim. Acta* **56**, 607–616.
- Mungall J. E. and Brenan J. M. (2003) Experimental evidence for the Chalcophile behavior of the halogens. *Can. Mineral.* **41**, 207–220.
- Nash W. P., Carmichael I. S. E. and Johnson R. W. (1969) The mineralogy and petrology of Mount Suswa, Kenya. *Earth Sci. Rev.* **10**, 409–439.
- Newman S. and Lowenstern J. B. (2002) VOLATILECALC: a silicate melt-H₂O-CO₂ solution model written in Visual Basic for excel. *Comput. Geosci.* **28**, 597–604.
- Norris C. A. and Wood B. J. (2017) Earth's volatile contents established by melting and vaporization. *Nature* **549**, 507–510.
- Pownceby M. I. and O'Neill H. S. C. (1994) Thermodynamic data from redox reactions at high temperatures. IV. Calibration of the Re-ReO₂ oxygen buffer from EMF and NiO + Ni-Pd redox sensor measurements. *Contrib. Mineral. Petrol.* **118**, 130–137.
- Prausnitz J. M., Lichtenthaler R. N. and Gomes De Azevedo E. (1999) Molecular thermodynamics of fluid-phase equilibria. 3rd ed. N. R. Amundson, Prentice Hall International series in the physical and chemical engineering sciences, New Jersey.
- Presnall D. C., Dixon S. A., Dixon J. R., O'Donnell T. H., Brenner N. L., Schrock R. L. and Dycus D. W. (1978) Liquidus phase relations on the join Diopside-Forsterite-Anorthite from 1 atm to 20 kbar. Their bearing on the generation and crystallization of basaltic magma. *Contrib. Mineral. Petrol.* **66**, 203–220.
- Robie R. A., Hemingway B. S. and Fisher J. R. (1979) Thermodynamic properties of minerals and related substances at 298.15 K and 1 bar (105 Pascals) pressure and at higher temperatures, Washington.
- Shannon R. D. (1976) Revised effective ionic radii and systematic studies of interatomic distances in halides and chalcogenides. *Acta Crystallogr.* **32**, 751–767.
- Sharp Z. D., Helffrich G. R., Bohlen S. R. and Essene E. J. (1989) The stability of sodalite in the system NaAlSi₃O₈-NaCl. *Geochim. Cosmochim. Acta* **53**, 1943–1954.
- Shinohara H., Iiyama J. T. and Matsuo S. (1989) Partition of chlorine compounds between silicate melt and hydrothermal solutions: I. Partition of NaCl-KCl. *Geochim. Cosmochim. Acta* **53**, 2617–2630.
- Signorelli S. and Carroll M. R. (2002) Experimental study of Cl solubility in hydrous alkaline melts: constraints on the theoretical maximum amount of Cl in trachytic and phonolitic melts. *Contrib. Miner. Petrol.* **143**, 209–218.
- Stelling J., Botcharnikov R. E., Beermann O. and Nowak M. (2008) Solubility of H₂O- and chlorine-bearing fluids in basaltic melt of Mount Etna at T = 1050–1250 °C and P = 200 MPa. *Chem. Geol.* **256**, 102–110.
- Stormer J. C. and Carmichael I. S. E. (1971) The free energy of sodalite and the behaviour of chloride, fluoride and sulfate in silicate magmas. *Am. Mineral.* **56**, 292–306.
- Takeda S., Nagata Y. and Kawakita Y. (2007) Slow dynamic properties of molten silver halides. *J. Non. Cryst. Solids* **353**, 3169–3173.
- Tsu Y., Suenaga H., Katsutoshi T. and Yutaka S. (1982) The velocity of ultrasound in molten bismuth, aluminium, silver and copper. *Trans. Japan Inst. Met.* **23**, 1–7.
- Vlach S. R. F., Salazar-Naranjo A. F., Torres-Corredor J. S., De Carvalho P. R. and Mallmann G. (2019) Calibration of high-temperature furnace assemblies for experiments between 200 and 600 MPa with end-loaded piston-cylinder apparatuses. *Brazilian J. Geol.* **49**.
- Webster J. D. (1992) Fluid-melt interactions involving Cl-rich granites: experimental study from 2 to 8 kbar. *Geochim. Cosmochim. Acta* **56**, 659–678.
- Webster J. D. (2004) The exsolution of magmatic hydrosaline chloride liquids. *Chem. Geol.* **210**, 33–48.
- Webster J. D., Baker D. R. and Aiuppa A. (2018) Halogens in Mafic and Intermediate-Silica Content Magmas. In *The Role of Halogens in Terrestrial and Extraterrestrial Geochemical Processes* (eds. D. E. Harlov and L. Aranovich). pp. 307–430.
- Webster J. D. and Holloway J. R. (1988) Experimental constraints on the partitioning of Cl between topaz rhyolite melt and H₂O and H₂O + CO₂ fluids: new implications for granitic differentiation and ore deposition. *Geochim. Cosmochim. Acta* **51**, 2091–2105.
- Webster J. D., Kinzler R. J. and Mathez E. A. (1999) Chloride and water solubility in basalt and andesite melts and implications for magmatic degassing. *Geochim. Cosmochim. Acta* **63**, 729–738.
- Webster J. D., Vetere F., Botcharnikov R. E., Goldoff B., McBirney A. and Doherty A. L. (2015) Experimental and modeled chlorine solubilities in aluminosilicate melts at 1 to 7000 bars and 700 to 1250 °C: Applications to magmas of Augustine Volcano, Alaska. *Am. Mineral.* **100**, 522–535.
- Webster J. D. and De Vivo B. (2002) Experimental and modeled solubilities of chlorine in aluminosilicate melts, consequences of magma evolution, and implications for exsolution of hydrous chloride melt at Mt. Somma-Vesuvius. *Am. Mineral.* **87**, 1046–1061.
- Wellman T. R. (1969) The vapor pressure of NaCl over decomposing sodalite. *Geochim. Cosmochim. Acta* **33**, 1302–1303.
- Wood B. J., Smythe D. J. and Harrison T. (2019) The condensation temperatures of the elements: a reappraisal. *Am. Mineral.* **104**, 844–856.
- Zimova M. and Webb S. (2006) The effect of chlorine on the viscosity of Na₂O-Fe₂O₃-Al₂O₃-SiO₂ melts. *Am. Mineral.* **91**, 344–352.

Associate editor: Bernard Charlier